Inorganic Chemistry Communications 47 (2014) 138–143

Contents lists available at ScienceDirect

Inorganic Chemistry Communications

journal homepage: www.elsevier.com/locate/inoche

The photovoltaic performance of dye-sensitized solar cells enhanced by using Dawson-type heteropolyacid and heteropoly blue-TiO_2 composite films as photoanode

Li Chen, Xiao-Jing Sang, Jian-Sheng Li, Chun-Hui Shan, Wei-Lin Chen *, Zhong-Min Su, En-Bo Wang *

Key Laboratory of Polyoxometalate Science of Ministry of Education, Department of Chemistry, Northeast Normal University, Changchun, Jilin 130024, China

ARTICLE INFO

Article history:
Received 24 June 2014
Received in revised form 15 July 2014
Accepted 16 July 2014
Available online 17 July 2014

Keywords:
Heteropolyacid
Heteropoly blue
Photoanode
Dye-sensitized solar cells

ABSTRACT

Dawson-type heteropolyacid $\{P_2Mo_{18}^{VI}\}$ and its two-electron heteropoly blue $\{P_2Mo_2^{V}Mo_{16}^{VI}\}$-doped TiO_2 composites have been successfully prepared by a simple sol–gel method and introduced into the photoanode of dye-sensitized solar cells (DSSCs), which results in a significant performance enhancement of DSSCs. The electrochemical impedance spectroscopy (EIS) and open-circuit voltage decay (OCVD) curve were employed to investigate the electron transport and carrier recombination behavior in DSSCs. The results show that doping with $\{P_2Mo_{18}^{VI}\}$ and $\{P_2Mo_2^{V}Mo_{16}^{VI}\}$ could both suppress the dark current and increase the electron lifetime in DSSCs. The performance of DSSCs with both $\{P_2Mo_{18}^{VI}\}$-doped and $\{P_2Mo_2^{V}Mo_{16}^{VI}\}$-doped photoanodes is better than that with pure P25 photoanodes and the overall conversion efficiency was improved by 24.48% and 17.19%, respectively.

In recent years, with the growing requirements of clean energy, solar energy has become the most alternative. The dye-sensitized solar cells (DSSCs) have been widely studied for decades due to their high efficiency, low-cost, eco-friendly production and great application prospect. Since 1991, M. Grätzel and O'Regan firstly reported DSSCs, the highest photoelectric conversion efficiency has been more than 15% [1–4]. Generally, DSSCs consist of the following components: a sensitized photoanode which is typically a dye-sensitized TiO_2 film on fluorine-doped tin oxide, redox couple, and a counter electrode which is usually platinized FTO conducting glass [5]. In fact, photoanode, which is the most important component of the DSSCs owing to its influence on the adsorption quantity of dye and the electron transport, has been extensively studied by many groups. In order to improve the energy conversion efficiency of DSSCs, various methods have been reported, such as, employing different semiconductors (ZnO, Nb_2O_5, In_2O_3, and WO_3) to take the place of TiO_2 [6–10], metal-doped (Au-doped, W-doped, and Ta-doped TiO_2) [11–13], and nonmetal-doped (N-doped and B-doped TiO_2) [14,15].

As it is known to all, POMs, which are a class of metal oxygen clusters on the nanoscale with remarkable structural diversity and variety of chemical composition, have been widely applied in medicine, catalysis and material science [16–19]. In recent years, the application of POMs in the DSSCs has made some achievements and they have been applied for the various components of DSSCs. POMs have been acting as dye of DSSCs, which is a very key innovation [20]. POMs also have been used to act as pure-inorganic electron-transfer mediators on DSSCs [21] and the counter electrode is modified by POM-based multilayer film [22]. In addition, some groups also introduced the POMs into photoanode. POM-doped semiconductors can enhance the photocurrent and reduce the electron–hole recombination in DSSCs. For example, polyoxometalate–anatase TiO_2 composites are introduced into the photoanode of dye-sensitized solar cells to retard the recombination and increase the electron lifetime, and the results show that the overall improvement of the efficiency is 22.8% by using the polyoxometalate-based photoanode [23]. Wang et al. utilize a simple solvothermal route method to prepare ZnO nanoparticles containing $H_3PW_{12}O_{40}$, which improved the efficiency by 49.2% compared to that of without POMs [24]. Heteropoly blue (HPB), which is obtained by reducing heteropolyacids, shows a new absorption bands in visible light region. HPB has many excellent properties, which has been used as new efficient catalysts [25], corrosion-resistant coatings [26], materials for molecular [27] etc. However, photoactive research of HPB under visible light is only carried out in recent years. Majima et al. investigated the one-electron redox processes during polyoxometalate-mediated photocatalytic reactions of TiO_2 studied by two-color two-laser flash photolysis, and they found that the efficiency of the electron transfers from the CB of TiO_2 depending on the reduction potential (E_{red}) of the POMs [28].

To date, no one has introduced the Mo-containing Dawson-type heteropolyacid and HPB into the photoanode of DSSCs. The synthetic method of Mo-containing Dawson-type heteropolyacid and its HPB is

* Corresponding authors.
E-mail addresses: chenwl@nenu.edu.cn (W.-L. Chen), wangeb889@nenu.edu.cn, wangeb889@hotmail.com (E.-B. Wang).

http://dx.doi.org/10.1016/j.inoche.2014.07.019
1387-7003/

simple and cheap. Furthermore, Mo-containing HPB is relatively stable in the air [S1, S2]. So in this work, Dawson-type heteropolyacid $(NH_4)_8[P_2Mo^{VI}_{18}O_{62}]$ (denoted as $\{P_2Mo^{VI}_{18}\}$) and its HPB $(NH_4)_8[P_2Mo^{V}_2Mo^{VI}_{16}O_{62}]$ (denoted as $\{P_2Mo^{V}_2Mo^{VI}_{16}\}$) were both incorporated into TiO_2 nanocomposite by a similar sol–gel method as discussed in the literature [29]. The results show that $\{P_2Mo^{VI}_{18}\}$-doped and its HPB $\{P_2Mo^{V}_2Mo^{VI}_{16}\}$-doped photoanodes can both improve the performance of the DSSCs, and the performance of $\{P_2Mo^{V}_2Mo^{VI}_{16}\}$-doped is slightly better than $\{P_2Mo^{VI}_{18}\}$-doped.

The cyclic voltammetry of $\{P_2Mo^{V}_2Mo^{VI}_{16}\}$ and $\{P_2Mo^{VI}_{18}\}$ was carried out to investigate the electrochemical properties of POMs. As can be seen in Fig. 1, there are three couples of reversible redox peaks for both $\{P_2Mo^{V}_2Mo^{VI}_{16}\}$ and $\{P_2Mo^{VI}_{18}\}$, which are assigned to the continuous reduction processes of Mo centers in the framework of POMs. Because the lowest unoccupied molecular orbital (LUMO) of the POMs is formally a combination of *d* orbits centering on the metal atoms [30,31], the LUMO level of $\{P_2Mo^{V}_2Mo^{VI}_{16}\}$ and $\{P_2Mo^{VI}_{18}\}$ could be estimated by finding out the first reduction applied potential, which corresponds to +0.57 V and +0.59 V vs NHE, respectively. Experimental results show that the LUMOs of $\{P_2Mo^{V}_2Mo^{VI}_{16}\}$ and $\{P_2Mo^{VI}_{18}\}$ are both lower than the conduction band level of TiO_2 (−0.5 V vs NHE). So $\{P_2Mo^{VI}_{18}\}$ and $\{P_2Mo^{V}_2Mo^{VI}_{16}\}$ can both accept the trapping of photogenerated electrons in TiO_2, which renders $\{P_2Mo^{V}_2Mo^{VI}_{16}\}$ and $\{P_2Mo^{VI}_{18}\}$ the fundamental feasibility to be the potential useful electron attractor for photovoltaic application.

XRD was carried out to investigate the changes of TiO_2 phase structure after doping with $\{P_2Mo^{V}_2Mo^{VI}_{16}\}$ and $\{P_2Mo^{VI}_{18}\}$. The XRD patterns of pure TiO_2, $\{P_2Mo^{VI}_{18}\}$-doped, and $\{P_2Mo^{V}_2Mo^{VI}_{16}\}$-doped photoanodes are shown in Fig. 2. As can be seen from the results, the three photoanodes, and nine characteristic peaks are observed at ca. 25.4°, 37.9°, 48.2°, 54.3°, 55.2°, 62.9°, 69.0°, 70.0°, and 75.3°. All these peak positions are in agreement with those of anatase TiO_2 which has been reported in literature [29,32]. As can be seen from Fig. 2a, there are four additional added peaks at 7.7°, 9.5°, 14.2° and 17.2° for $\{P_2Mo^{V}_2Mo^{VI}_{16}\}$-doped photoanodes compared with those of TiO_2, which are assigned to $\{P_2Mo^{V}_2Mo^{VI}_{16}\}$ incorporated in photoanodes. Meantime, we can also find that the composition of $\{P_2Mo^{V}_2Mo^{VI}_{16}\}$ and TiO_2 makes the peaks at 14.2° and 17.2° become strong and the peaks at 7.7° and 9.5° become weak. In Fig. 2b, we can get the same results. Compared with pure TiO_2, four additional peaks can be found at 8.0°, 9.3°, 13.9° and 17.4° for $\{P_2Mo^{VI}_{18}\}$-doped TiO_2, which also appeared in the $\{P_2Mo^{VI}_{18}\}$. But the intensity of the peaks changed. Furthermore, we have also investigated the solid diffuse spectra of $\{P_2Mo^{V}_2Mo^{VI}_{16}\}$ and $\{P_2Mo^{VI}_{18}\}$-doped TiO_2 and pure P25 (in the Fig. S4). By comparison, we find that the absorption of $\{P_2Mo^{V}_2Mo^{VI}_{16}\}$-doped is stronger than those of $\{PMo^{VI}_{18}\}$-doped in the visible region, which results from the reason that HPB has a strong absorption band in the visible area. In Fig. S4b, we find that the absorption of $\{P_2Mo^{V}_2Mo^{VI}_{16}\}$-doped is obviously stronger than pure P25 in the visible region. The above results indicated that $\{P_2Mo^{V}_2Mo^{VI}_{16}\}$ and $\{P_2Mo^{VI}_{18}\}$ were successfully incorporated into TiO_2.

The SEM images were carried out to investigate the surface morphology, the dispersion and the size of particles in the as-prepared photoanodes. Fig. 3 shows the SEM images of the calcined pure P25,

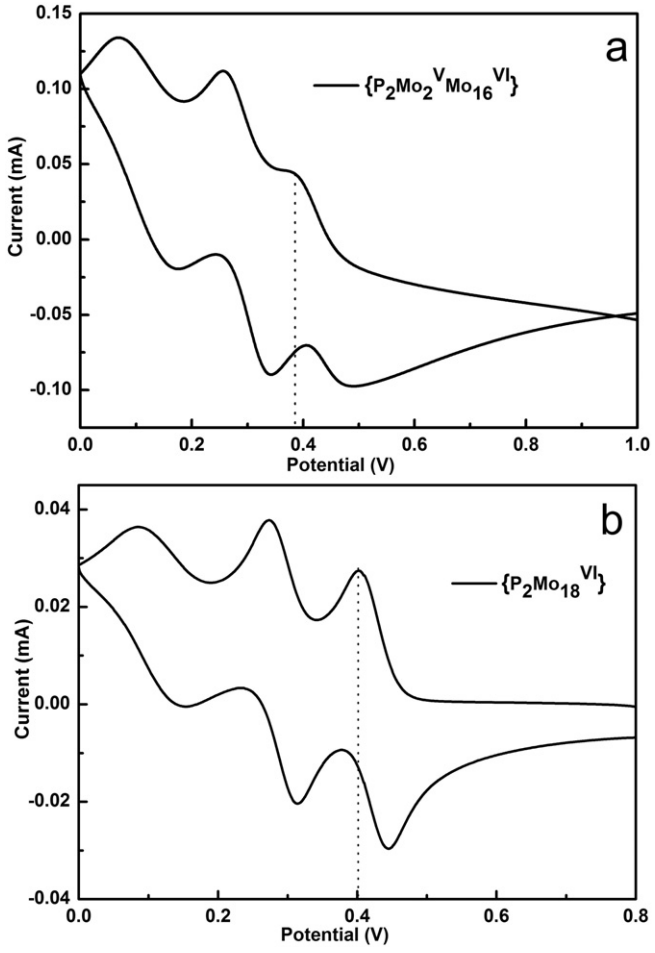

Fig. 1. Cyclic voltammetry curve of the $\{P_2Mo^{V}_2Mo^{VI}_{16}\}$ (a) and $\{P_2Mo^{VI}_{18}\}$ (b) in Na_2SO_4/H_2SO_4 buffer solution with pH = 1.3 in the voltage range from 0 V to 1.0 V.

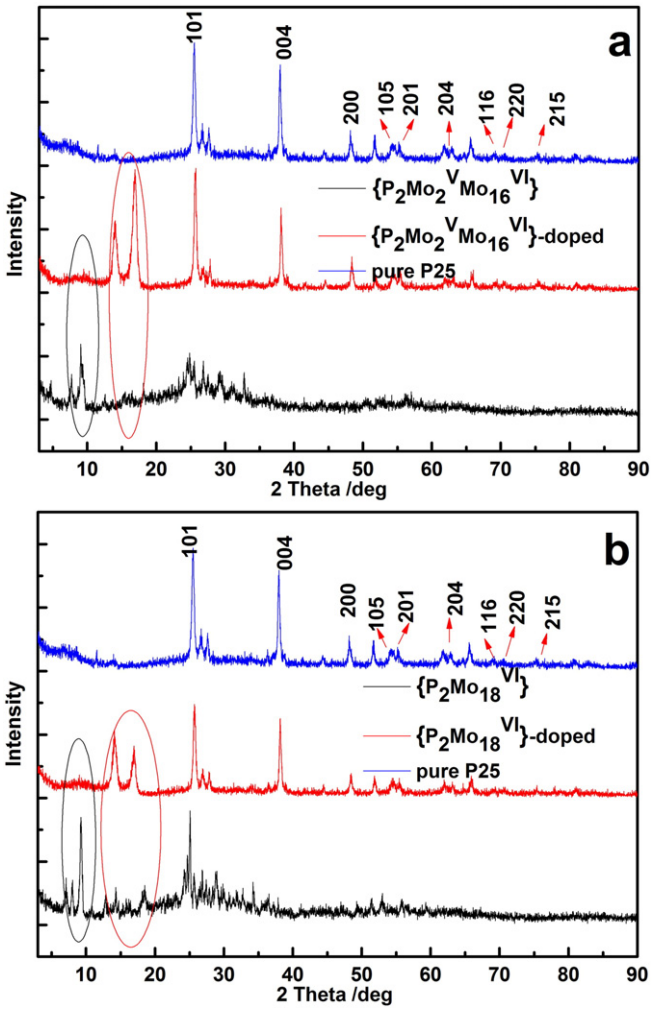

Fig. 2. XRD data of as-prepared photoanodes: (a) $\{P_2Mo^{V}_2Mo^{VI}_{16}\}$-doped, $\{P_2Mo^{V}_2Mo^{VI}_{16}\}$, pure P25; (b) $\{P_2Mo^{VI}_{18}\}$-doped, $\{P_2Mo^{VI}_{18}\}$ and pure P25.